ELSEVIER

Earth and Planetary Science Letters 144 (1996) 93–108

EPSL

Water in the oceanic upper mantle: implications for rheology, melt extraction and the evolution of the lithosphere

Greg Hirth [a,*], David L. Kohlstedt [b]

[a] *Department of Geology and Geophysics, Woods Hole Oceanographic Institution, Woods Hole, MA 02543, USA*
[b] *Department of Geology and Geophysics, University of Minnesota, Minneapolis, MN 55455, USA*

Received 11 January 1996; revised 22 July 1996; accepted 29 July 1996

Abstract

The influence of water on the dynamics of the oceanic upper mantle is re-evaluated based on recent experimental constraints on the solubility of water in mantle minerals and earlier experimental studies of olivine rheology. Experimental results indicate that the viscosity of olivine aggregates is reduced by a factor of ~ 140 in the presence of water at a confining pressure of 300 MPa and that the influence of water on viscosity depends on the concentration of water in olivine. The water content of olivine in the MORB source is estimated to be 810 ± 490 H/10^6 Si, a value greater than the solubility of water in olivine at a confining pressure of 300 MPa (~ 250 H/10^6 Si). We therefore conclude that the viscosity of the mantle in the MORB source region is 500 ± 300 times less than that of dry olivine aggregates. The dependence of the solubility of water in olivine on pressure and water fugacity is used in conjunction with other petrological constraints to estimate the depth at which melting initiates beneath mid-ocean ridges. These calculations indicate that melting begins at a depth of ~ 115 km, consistent with other geochemical observations. Owing to the relatively small amount of water present in the MORB source, only ~ 1–2% melt is produced in the depth interval between the water-influenced solidus and the dry solidus. A discontinuity in mantle viscosity can develop at a depth of ~ 60–70 km as a result of the extraction of water from olivine during the MORB melting process. In the mid-ocean ridge environment, the mantle viscosity at depths above this discontinuity may be large enough to produce lateral pressure gradients capable of focusing melt migration to the ridge axis. These observations indicate that the base of an oceanic plate is defined by a compositional rather than thermal boundary layer, or at least that the location of the thermal boundary layer is strongly influenced by a compositional boundary, and that the evolution of the oceanic upper mantle is strongly influenced by a viscosity structure that is controlled by the extraction of water from olivine at mid-ocean ridges.

Keywords: mantle; water; dunite; rheology; viscosity; lithosphere

1. Introduction

The solubility of water in basalt is considerably higher than that in olivine, leading Karato [1] to propose that partial melting may increase the viscosity of the mantle if the retained melt fraction remains small. Results from recent deformation experiments on partially molten olivine aggregates deformed with or without added water support this hypothesis [2]. At the same time, analysis of the water content of both natural and experimentally annealed crystals has demonstrated that significant amounts of water

* Corresponding author. E-mail: ghirth@whoi.edu

PII S0012-821X(96)00154-9

can be stored in 'nominally anhydrous' minerals such as olivine and pyroxenes in the upper mantle (e.g., [3–5]).

In this paper we use constraints provided by experimental studies on the rheological properties of olivine aggregates and the solubility of water in mantle minerals to: (1) re-evaluate the influence of water on the viscosity of olivine aggregates: (2) calculate the amount of water dissolved in olivine in the mid-ocean ridge basalt (MORB) source region: (3) estimate the depth at which melting initiates beneath mid-ocean ridges; (4) evaluate how the depletion of water resulting from melt extraction influences the viscosity structure of the oceanic upper mantle; and (5) calculate viscosity profiles for the oceanic upper mantle as a function of age using standard assumptions for the evolution of the thermal structure of the lithosphere. The results of these analyses are used to discuss the role of water on the formation of oceanic plates, melt extraction at mid-ocean ridges and the depth distribution of seismic anisotropy in the oceanic mantle.

Throughout the manuscript we assume that the viscosity of the mantle can be determined from the rheological behavior of olivine aggregates (dunites). The rheological properties of olivine aggregates determined from deformation experiments are described using a flow law of the form:

$$\dot{\epsilon} = A\sigma^n \exp\left(\frac{-(Q+PV)}{RT}\right) \quad (1)$$

where $\dot{\epsilon}$ is strain rate, A is a material parameter, σ is differential stress, Q is an activation energy, P is pressure, V is an activation volume, R is the ideal gas constant, and T is absolute temperature. Following Karato and Wu [6] we report effective viscosities at a constant stress using the relationship:

$$\eta = \frac{\sigma}{\dot{\epsilon}} = \frac{A^{-1}}{\sigma^{n-1}} \exp\left(\frac{Q+PV}{RT}\right) \quad (2)$$

We do not account for the role of pyroxenes and garnet/spinel. Theoretical and experimental studies demonstrate that this assumption is reasonable. For example, while the predominant secondary mineral in peridotites (orthopyroxene) may be up to 25% stronger than olivine [7], numerical models indicate that an aggregate comprised of 60% olivine and 40% orthopyroxene would only be ~ 7.5% stronger than pure dunite for deformation in the dislocation creep regime [8]. Similarly, deformation experiments on fine-grained lherzolites in both the diffusion and dislocation creep regimes show that the presence of pyroxene and spinel does not significantly increase the strength of peridotite relative to that of dunite [9]. Therefore, neglecting the effect of the other mantle minerals should result in no more than a factor of ~ 1.3 (i.e., 1.075^n where n the stress exponent is ~ 3.5) underestimation of viscosity.

2. Water weakening of olivine aggregates

It has been known since at least the early 1970s that the presence of water reduces the strength of olivine aggregates [10–12]. Unfortunately, a number of experimental complications have made quantification of the water weakening effect difficult, including the relatively poor resolution of mechanical data obtained using a solid-media deformation apparatus, difficulty in controlling the chemical environment within sample assemblies, and complexities that arise due to partial melting of specimens during an experiment. However, several recent studies on the rheological and chemical properties of olivine aggregates provide a basis to re-evaluate the influence of water on the viscosity of olivine aggregates in the mantle.

Deformation experiments on intact cores of natural dunite demonstrate that the viscosity of olivine aggregates deformed in the dislocation creep regime is reduced by up to a factor of 180 in the presence of water at a confining pressure of 300 MPa. Mechanical data from the studies of Chopra and Paterson [11,13], abbreviated as C and P, are shown in Fig. 1a; following C and P, data for 'wet' samples are separated into two groups according to whether the starting material was Anita Bay or Aheim dunite. In both cases, the water present during deformation came from dehydration of alteration phases in the starting materials. To ensure that all of these data represent steady state deformation by dislocation creep and not a combination of brittle and plastic processes, only data for experiments with strengths less than 300 MPa were used. Because all of C and P's experiments were conducted at a confining pressure of 300 MPa, it is likely that semi-brittle pro-

cesses partly influenced the rheology of the samples at differential stresses greater than ~ 300 MPa (e.g., [14]). Before plotting the data on an Arrhenius plot, we examined the edited C and P data set to re-evaluate the stress exponent (n) determined under wet conditions. Whereas C and P conducted a global inversion of the data set to determine n, we determined n using least-squares linear fits of data from samples deformed at the same temperature. This simplified data reduction technique reduces uncertainties arising from partial melting of the samples (e.g., differences in the amount of melt present and the partitioning of water between solid and melt phases). A least-squares fit to the data from 10 'wet' Anita Bay samples deformed at 1200°C yields an n of 3.4 ± 0.2; within error, this value is the same as that determined for dry samples of both Aheim and Anita Bay dunite ($n = 3.6 \pm 0.2$).

The Arrhenius plot in Fig. 1a was constructed by normalizing the edited C and P data set to a differential stress of 200 MPa using $n = 3.5$. A value of $n = 3.5$ (instead of 3.4 or 3.6) was used based on the observation that $n = 3.5 \pm 0.1$ for olivine single crystals deformed in different orientations and chemical environments [15]. Least-squares linear fits of the 'wet' Anita Bay data yield an activation energy of 515 ± 25 kJ/mol; this value is also indistinguishable from that determined for dry samples of both Anita Bay and Aheim dunite. A comparison of the data from dry samples to that from the Anita Bay dunite demonstrates that the presence of water results in a factor of 180 increase in creep rate (i.e., a factor of 180 decrease in viscosity) at a constant stress. As described below, we suggest that the data for Aheim dunite fall below the 'wet' fit because the aggregate becomes undersaturated with water due to the presence of melt.

The influence of water on the viscosity of olivine single crystals determined by Mackwell et al. [16] is

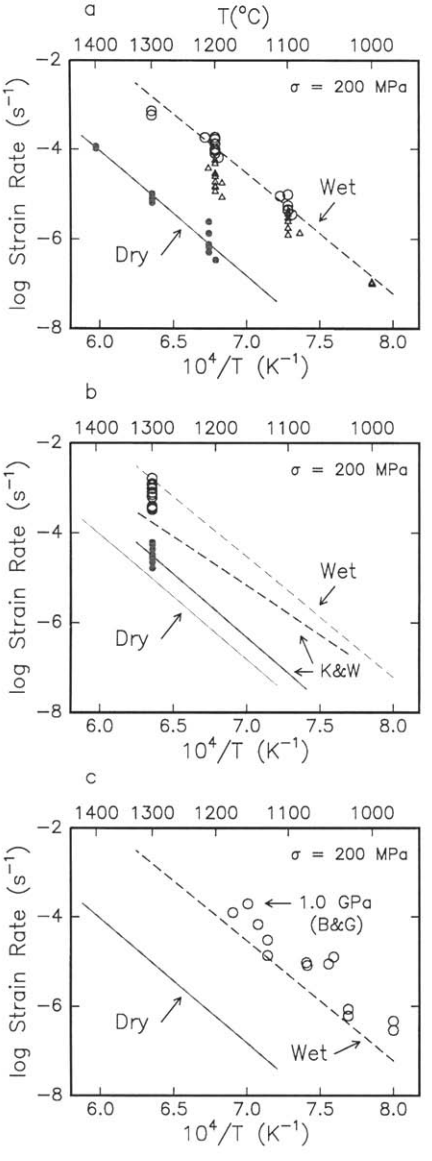

Fig. 1. Experimental data illustrating the influence of water on the viscosity of olivine aggregates. (a) Plot of log strain rate versus inverse temperature demonstrating that the presence of water results in up to a factor of 180 decrease in viscosity at a confining pressure of 300 MPa; data from Chopra and Paterson [11,13] are plotted based on a re-evaluation of the stress exponent. ● = data for dry samples of both Anita Bay and Aheim dunite; ○ = data for wet Anita Bay dunite; triangles = data for wet Aheim dunite; dashed line = least-squares fit to the data for wet Anita Bay samples; solid line = the dry olivine flow law of Chopra and Paterson [11]. (b) Plot of log strain rate versus inverse temperature for the dry (●) and wet (○) samples of Karato et al. [12]. The bold lines labelled K and W are flow laws from Karato and Wu [6]. The data were corrected to a stress of 200 MPa using $n = 3.5$. The lines labelled Dry and Wet are the same as those shown in (a). (c) Plot of log strain rate versus inverse temperature comparing the revised Chopra and Paterson flow laws (labelled Wet and Dry) with data from Borch and Green [18] obtained at a confining pressure of 1.0 GPa; the data were corrected to a stress of 200 MPa using $n = 3.5$.

somewhat smaller than that indicated by Fig. 1a. However, the single crystal data may only provide a minimum estimate of the influence of water on viscosity. Comparison of mechanical data from experiments on olivine aggregates and single crystals indicates that the rheology of coarse-grained olivine aggregates (i.e., at conditions far from the diffusion creep regime) is controlled by slip on (010)[001], the hardest of the dominant slip systems (e.g., [11–13,17]). Single crystals oriented to favor slip on (010)[001] are a factor of 3–3.5 weaker in the presence of water [16]. With a stress exponent of 3.5, these data correspond to a factor of 50–80 decrease in viscosity. However, continuous hardening, observed during the wet experiments conducted at the slowest strain rates, suggests that the samples were drying out during deformation. Indeed, the water contents of these deformed single crystals [16] are approximately a factor of two less than those of samples hydrostatically annealed at the same pressure [16,4]. Apparently, the single crystals were not saturated with water during deformation and thus provide only a minimum estimate for the magnitude of weakening.

The influence of water on viscosity obtained from experiments on hot-pressed olivine aggregates produced from powders with a grain size of ~ 10 μm [12] and by the dislocation creep flow laws of Karato and Wu [6] is also smaller than that shown in Fig. 1a. As demonstrated in Fig. 1b, the viscosity of Karato et al. [12] dry samples is somewhat lower than predicted by the C and P dry flow law, while that of Karato et al. wet samples is slightly greater than predicted by the revised C and P wet flow law. Karato et al. only conducted experiments at 1300°C. There are at least two reasons for the lower viscosity exhibited by Karato et al. dry samples: (1) some of their 'dry' samples contained small amounts of water [12], and (2) their experiments were conducted at conditions near the transition from dislocation to diffusion creep. Subsequent experiments on fine-grained olivine aggregates indicate that a transition from (010)[001] to (010)[100] controlled creep occurs near the transition from diffusion to dislocation creep [17]; the change in controlling slip system can result in as much as an order of magnitude decrease in viscosity. Karato et al. wet samples display a slightly higher viscosity than our revised C and P flow law. The mean strain rate of Karato et al. wet data shown in Fig. 1b is approximately a factor of 2 lower than that of the modified C and P flow law at 1300°C. Thus, at a minimum, the presence of water reduces the viscosity of olivine aggregates by a factor of ~ 100. The dislocation creep flow laws of Karato and Wu [6] underestimate the influence of water on viscosity, as shown in Fig. 1b.

Several observations suggest that the influence of water on viscosity depends on the concentration of water in olivine. A comparison of the revised C and P flow law to data collected at 1.0 GPa using a liquid-medium apparatus [18] is shown in Fig. 1c. The higher pressure data yield a viscosity approximately 3 times lower than the revised C and P flow law. Similarly, as shown in Fig. 2a, the solubility of water in olivine increases by a factor of ~ 3 with an increase in pressure from 0.3 to 1.0 GPa [19]. Although Borch and Green [18] reported that their samples were dry, subsequent analysis of the same starting material by FTIR [20] demonstrates that there was enough water to saturate the olivine at 1.0 GPa. Additional evidence for concentration-dependent water weakening comes from the single crystal experiments described above [16]. The 'wet' single crystals deformed at 1300°C and a strain rate of 10^{-5} s^{-1} all continuously hardened at finite strains well above that required to achieve steady-state deformation under dry conditions at a strain rate of 10^{-5} s^{-1} or under wet conditions at strain rates $\geq 10^{-4}$ s^{-1}. The continuous hardening therefore implies that the samples were drying out, so that the strength was increasing due to the loss of water.

Under hydrous conditions, the presence of melt can either reduce or increase the viscosity of olivine aggregates depending on the deformation mechanism, melt fraction, partitioning of water between solid and melt phases, and water content of the assemblage. Melt-induced reductions in viscosity occur due to a decrease in the area of grain to grain contact with increasing melt fraction. At the same time, melt-induced increases in viscosity can occur due to preferential partitioning of water into the melt (e.g., [1]). The solubility of water in basaltic melt is ~ 2500 times greater than that in olivine at a confining pressure of 300 MPa [4,21,22]. Thus, even small amounts of melt can significantly decrease the concentration of water in the solid assemblage. Because

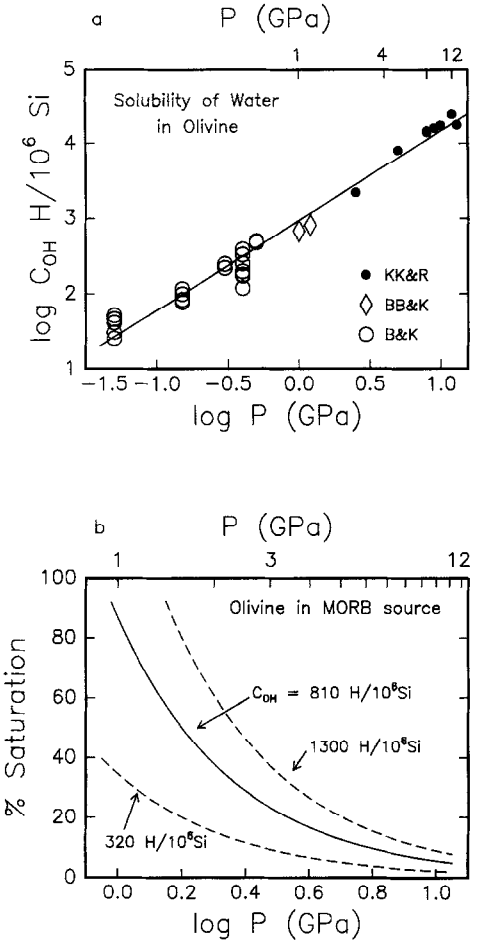

Fig. 2. (a) Plot of log solubility of water in olivine as a function of log pressure. KK&R = results from [5]; BB&K = unpublished results of Bai, Bai and Kohlstedt (see [5]); B&K = results from [4]. (b) Percent saturation of olivine with water in the MORB source versus log pressure (i.e., depth). The curves were calculated for three different estimates of the water content of olivine prior to the onset of melting.

the viscosity of olivine aggregates apparently depends on the concentration of water in olivine, the initiation of melting can result in an increase in viscosity. The effect of melt-induced changes in the distribution of water on the viscosity of partially molten olivine aggregates is illustrated by deformation experiments conducted in the diffusion creep regime [2,23]. Specifically, the strength of dunites with 8% melt is approximately the same with or without added water (0.2 wt%).

The difference in rheological behavior illustrated for Anita Bay and Aheim dunites in Fig. 1a can also be explained by melt-induced changes in the water content of olivine. Melt is present in both of these dunites deformed at these temperatures [13]. In fact, subsequent microstructural observations reveal between a few and 10 vol% melt in the Aheim dunite deformed at 1200°C [24]. Several observations indicate that the amount of melt produced in Aheim dunite, and therefore the likelihood of producing undersaturated olivine, is greater than that in Anita Bay. TEM microscopy shows that the melt in both materials is associated with dehydration (during the experiment) of hydrous silicates present along grain boundaries [11,24]. The total water content measured for both dunites is approximately the same after 'wet' experiments. However, because the Aheim initially contains ~2.5 times more (2 versus 5 vol%) hydrous silicates along grain boundaries [11] it is expected to contain more melt. This interpretation of the combined effects of melt and water on the rheology of olivine aggregates deformed at hypersolidus conditions provides further support for the hypothesis that the viscosity of olivine aggregates depends on the concentration of water in olivine.

Measurement of the spacing between subgrain boundaries in samples of 'wet' Aheim and 'wet' Anita Bay dunite provides additional support for our interpretation that the difference in viscosity of these rocks arises from differences in concentration of water in olivine. TEM analysis of dislocation structures in deformed single crystals indicates that the presence of water enhances the formation of subgrain boundaries [16]. Some question remains as to what degree this enhancement is related to differences in the magnitude of differential stress during experiments. Nonetheless, subsequent analysis of the dunites deformed by C and P demonstrates that the subgrain spacing in samples deformed at the same differential stress is smaller in the presence of water [25]. In addition, the subgrain spacing in 'wet' Aheim dunite is intermediate between that in wet Anita Bay and dry Anita Bay or Aheim dunite. This observation is consistent with the hypothesis that olivine grains in the 'wet' Aheim dunite contain less water than those in the 'wet' Anita Bay dunite.

In summary, we conclude that the viscosity of water-saturated olivine aggregates is 100–180 times

lower than that of dry aggregates at a confining pressure of 300 MPa, and that the influence of water on viscosity depends on the concentration of water in olivine. In the subsequent analysis of mantle rheology we assume that the viscosity of olivine aggregates is inversely proportional to water content such that viscosity is reduced by a factor of 140 at a water content of 250 $H/10^6$ Si (i.e., the solubility of water at 300 MPa).

3. Water in olivine in the oceanic mantle

The influence of water on the viscosity of the oceanic mantle depends on the amount of water present in the MORB source region and the amount of this water dissolved in olivine. Estimates for the amount of water present in the MORB source have been reported based on the water content of MORB and a comparison of the variation of its concentration with the abundances of other incompatible elements (e.g., [26–28]). Such geochemical analyses demonstrate that 'primary' MORB contains $\sim 0.1 \pm 0.05$ wt% H_2O and suggest a bulk partition coefficient during melting of ~ 0.01. Because MORB is produced by $\sim$ 10–20% melting of peridotite, the water content of MORB indicates that there is $\sim 125 \pm 75$ wt ppm H_2O in the MORB source. This estimate agrees well with independent calculations of the water content in the MORB source based on the amount of water measured in mantle minerals from xenoliths [3], as well as from measurements of electrical conductivity in the Pacific upper mantle [29].

The amount of the water in the MORB source that is dissolved in olivine depends on the partitioning of water among the mantle minerals. In the following analysis, we assume that all of the water resides in a melt-free peridotite consisting of olivine, low-Ca pyroxene (opx), high-Ca pyroxene (cpx) and garnet. The partition coefficients for water between these minerals, summarized in Table 1, were estimated using the following constraints:

1. the concentration of water in hydrothermally annealed olivine [4,5] and cpx [30] increases approximately as fH_2O^1;
2. the concentration of water in hydrothermally annealed cpx is a factor of 5–10 times greater than in olivine at pressures from 50 to 300 MPa [30];
3. the concentration of water in natural cpx is approximately a factor of two greater than in coexisting opx [3];
4. the concentration of water in natural opx and coexisting hydrous basaltic glass corresponds to a partition coefficient of 0.003–0.004 [31];
5. a comparison of the solubility of water in experimentally annealed olivine [4] and basaltic melt (e.g, [21,22]) at a pressure of ~ 300 MPa indicates a partition coefficient of ~ 0.0004;
6. the concentration of water in natural garnets is similar to that in coexisting olivine [3].

Table 1
Partition coefficients for water in mantle minerals

Mineral pair	D_{OH} (olivine–mineral)
olivine–opx	0.2
olivine–cpx	0.1
olivine–garnet	1

By employing the partition coefficients summarized in Table 1 for a mantle with 56% olivine, 19% opx, 10% cpx and 15% garnet (i.e., garnet pyrolite), the geochemically constrained value for the water content of the MORB source indicates that the olivine in this assemblage contains 810 ± 490 $H/10^6$ Si ($\sim 50 \pm 30$ wt ppm) water. The lower estimate of ~ 320 $H/10^6$ Si is greater than the solubility of water in olivine at a pressure of 300 MPa. Thus, these mass balance calculations indicate that the water content in the MORB source is more than sufficient to induce the full viscosity reduction observed for olivine aggregates deformed under hydrous conditions at a pressure of 300 MPa in the laboratory (i.e., a reduction in viscosity by a factor of ~ 140). Assuming that the viscosity of olivine aggregates is inversely proportional to water content, the estimate of 810 ± 490 $H/10^6$ Si yields a viscosity of the mantle in the MORB source that is 500 ± 300 times lower than that of dry olivine aggregates at the same temperature and pressure.

4. Depth of melting beneath mid-ocean ridges

Because the solubility of water in melt is two to three orders of magnitude greater than that in mantle minerals, the MORB melting process can effectively

'dry out' the mantle. The implications of this drying out process on the viscosity of the oceanic mantle depend on the depth at which melting initiates. This depth can be calculated from the estimates of the water content of olivine in the MORB source combined with the experimentally determined solubility of water in olivine; the solubility of water in olivine as a function of pressure is shown in Fig. 2a. A plot of the percent saturation of water in olivine (and thus in the mantle assemblage) versus pressure is shown in Fig. 2b. This plot was produced by dividing the estimate for the amount of water dissolved in olivine in the MORB source (810 H/10^6 Si) as well as the upper (1300 H/10^6 Si) and lower (320 H/10^6 Si) estimates by the solubility of water shown in Fig. 2a at the appropriate pressure. Fig. 2b illustrates that a mantle assemblage containing olivine with 810 H/10^6 Si would be ~ 50% saturated with water at a depth of ~ 50 km (i.e., a pressure of 1.7 GPa).

The information in Fig. 2b can be used to predict the depth at which melting initiates by considering how much the peridotite solidus is lowered under hydrous, but undersaturated, conditions. Experimentally constrained estimates for the dry [32] and wet [33] peridotite solidi as a function of pressure are presented in Fig. 3. In addition, peridotite solidi for water-undersaturated conditions are shown as dotted lines with 'contour intervals' corresponding to 0.1 increments in the activity of water (a_{H_2O}). Experimental data on the influence of water on the solidus temperature of peridotite for water-undersaturated conditions are lacking. Therefore, the a_{H_2O} contours are somewhat schematically located in Fig. 3, motivated by the relationship between solidus temperature and a_{H_2O} determined for the albite–water system [21]. The percent saturation curves shown in Fig. 2b are also plotted as 'solidi' in Fig. 3. These curves were mapped onto the phase diagram by assuming that the activity coefficient for water in olivine is unity. For comparison with Fig. 2b, notice that the solidus curve for a mantle assemblage containing olivine with 810 H/10^6 Si water crosses the a_{H_2O} = 0.5 contour at a pressure of ~ 1.7 GPa. The depth of the onset of melting can be estimated from this plot by noting the pressure at which the mantle adiabat crosses the appropriate solidus. The adiabat crosses the solidus for a mantle assemblage containing olivine with 810 H/10^6 Si at a pressure of ~ 3.7 GPa,

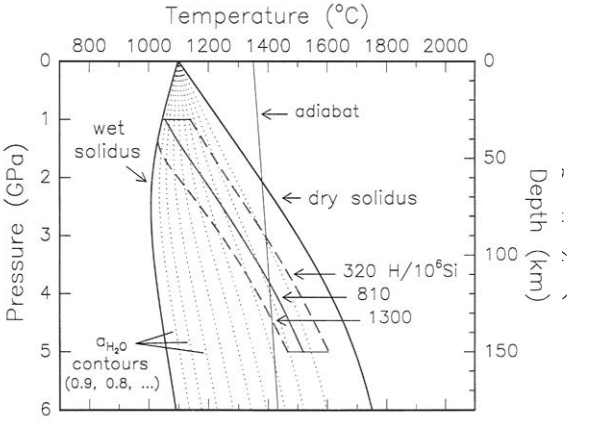

Fig. 3. Temperature–pressure phase diagram illustrating the depth at which melting initiates beneath a mid-ocean ridge. The bold solid and dashed lines are solidi for mantle assemblages containing olivine with 810, 810+490 and 810–490 H/10^6 Si. The location of the solidi for different values of a_{H_2O} are indicated by dotted lines. The intersection of the mantle adiabat with the solidus for an assemblage containing olivine with 810 H/10^6 Si indicates that melting initiates at a depth of ~ 115 km beneath mid-ocean ridges.

indicating that melting initiates at a depth of ~ 115 km beneath the mid-ocean ridges. As shown in Fig. 3, the depth of this 'water-influenced' solidus ranges from ~ 80 to 150 km for a MORB source with 320 and 1300 H/10^6 Si in olivine, respectively, and a ±50°C variation in the temperature of the mantle adiabat.

In producing Fig. 3, we have assumed that the influence of the CO_2 on the solidus in the mid-ocean ridge environment is negligible. The shortcoming of this assumption is that phase equilibrium experiments demonstrate that, above ~ 2 GPa, carbonate phases become stable in CO_2-saturated mantle assemblages. Thus, because the temperature in the oceanic mantle is presumably above the decarbonation temperature for a high-pressure carbonate phase, a small amount of carbonitic melt may be present in the MORB source (e.g., [34]). The implications of such a melt phase are discussed further below.

The estimate of depth for the onset of melting determined from Fig. 3 provides another solution for the apparent paradox indicated by geochemical analyses that require MORB melting in the garnet lherzolite facies (see also [35]). While analyses of the major element composition of MORB indicate that

melting initiates at depths of ~ 60–70 km [36,37], measurement of trace element ratios in MORB, such as Hf/Lu or U/Th, indicate that melting initiates at a depth where garnet is a stable phase (e.g., [38,39] and references therein). Melting could initiate in the garnet facies if the mantle temperature were high enough to induce 'dry melting' at ~ 100 km. However, in that case, extreme degrees of melting would occur [32,36]. Although our analysis suggests that the water content of the MORB source can influence the depth at which melting initiates, there is not enough water to increase dramatically the total amount of melt produced at mid-ocean ridges. Thus, the initiation of melting at a 'volatile-influenced' solidus provides a mechanism for producing a garnet signature in MORB without extreme degrees of melting. For further discussion on the role of volatile-induced melting in the generation of MORB see Plank and Langmuir [40] and references therein.

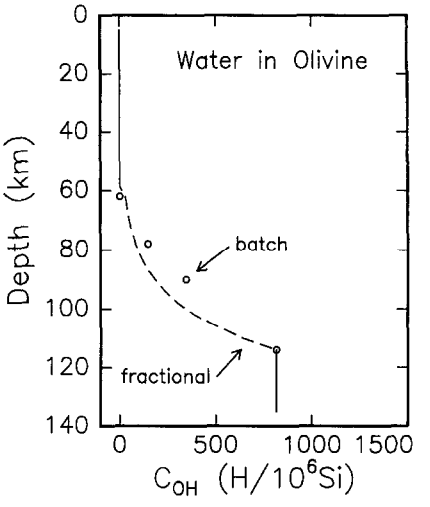

Fig. 4. Water content of olivine versus depth beneath a mid-ocean ridge. The change in water content is shown for both fractional and batch MORB melting scenarios.

5. The wet-to-dry transition

The arguments presented above indicate that small amounts of melt can be produced at depths between ~ 115 and 60 km beneath mid-ocean ridges. The influence of this melt on the viscosity of the mantle depends on how the melting process affects the concentration of water in olivine. Consequently, the effect of the onset of melting on the viscosity of the upper mantle depends on the melt fraction at which the melt phase becomes interconnected (and therefore mobile) and whether the melting process proceeds in a batch or fractional manner.

Theoretical considerations indicate that vanishingly small melt fractions are interconnected if the dihedral angle between the melt and solid residue is $< 60°$ (e.g., [41]). Experimental observations in the olivine–basalt system show mean dihedral angles ($\sim 40°$ [41]) and transport properties [42] that indicate that melt is interconnected at melt fractions less than 0.005. However, because melting presumably occurs along multi-phase grain boundaries, it is important to consider the wetting characteristics of basaltic melt and the other mantle minerals. The issue of whether basaltic melt 'wets' three-grain edges of pyroxenes remains unresolved [43]. There are indications that the presence of water reduces the dihedral angle between pyroxenes and basalt (see [43]). Thus, because the initial melt will contain a considerable amount of water, it will likely be interconnected at a very low melt fraction. This hypothesis is consistent with geochemical observations that indicate that low-degree partial melts must be extracted from the garnet lherzolite facies and transported to shallow depths without significant equilibration with the low-pressure assemblage (e.g., [39], and references therein).

Several geochemical observations indicate that the MORB melting process involves at least some component of fractional melting (e.g., [44]). In addition, if melt flow becomes localized, due to a reactive–infiltration instability [45,46] or perhaps the development of a 'fractal root system' [39], then the small degrees of melt produced at ~ 100 km may be separated from the mantle residue very early in the melting process.

Estimates for the decrease in water content of olivine with decreasing depth are shown for both batch and fractional melting scenarios in Fig. 4; these relationships were calculated assuming that the initial water content of olivine was 810 H/10^6 Si. The change in the water content of olivine during batch melting was determined using relationships shown in Fig. 2 and Fig. 3. Over the depth interval between where the mantle adiabat crosses the 810

$H/10^6$ Si solidus and where it crosses the dry solidus (Fig. 3), the a_{H_2O} is estimated by noting the a_{H_2O} contour that the adiabat intersects at each depth. The corresponding water content of olivine is calculated using the solubility data in Fig. 2a, assuming that the percent saturation of the mantle assemblage can be directly related to a_{H_2O}. For example, at a depth of 92 km (a pressure of 3.1 GPa) the mantle adiabat crosses the $a_{H_2O} = 0.1$ contour. At a pressure of 3.1 GPa the solubility of water in olivine is ~ 3600 $H/10^6$ Si, indicating that olivine that is 10% saturated with water at a depth of 92 km beneath a mid-ocean ridge would contain ~ 360 $H/10^6$ Si.

The decrease in the water content of olivine associated with fractional melting was calculated using the relationships outlined in Appendix A. The values of D_{OH} *(i–melt)*, the distribution coefficient for water between the ith solid phase and melt, can be calculated from the distribution coefficients listed in Table 1 if D_{OH} *(ol–melt)* is known. As noted above, experimental data for the solubility of water in olivine and MORB indicate that D_{OH} *(ol–melt)* ≈ 0.0004 at a pressure of 300 MPa. However, because the solubility of water in olivine increases as $(f_{H_2O})^1$ while that of water in MORB increases as $(f_{H_2O})^{1/2}$, D_{OH} *(ol–melt)* increases with increasing pressure. The difference in the effect of f_{H_2O} is particularly significant for determining the water content of olivine in the MORB source because the fugacity coefficient for water increases rapidly at pressures greater than ~ 1.0 GPa [47].

An estimate for D_{OH} *(ol–melt)* at the depths where MORB melting initiates can be calculated using constraints provided by the experimental data for the solubility of water in olivine. The analysis outlined in the appendix yields D_{OH} *(ol–melt)* ≈ 0.003. The curve labelled fractional in Fig. 4 was calculated using Eq. (A1) employing D_{OH} *(ol–melt)* $= 0.003$ and the distribution coefficients listed in Table 1 to calculate D_{OH} *(solid–melt)* from Eq. (A2); in this case D_{OH} *(solid–melt)* ≈ 0.01.

The melt production rate in the water-influenced melting interval between the 810 $H/10^6$ Si solidus and the dry solidus was determined by assuming that all of the melt is produced as a result of the presence of water. As described above, the phase diagram in Fig. 3 indicates that the water content of the olivine decreases from ~ 810 to 360 $H/10^6$ Si over the depth interval from 115 to 92 km. Based on mass balance calculations with D_{OH} *(ol–melt)* $= 0.003$, such a change in water content corresponds to a melt production rate of $\sim 1\%/20$ km. The similarity of the two water content curves in Fig. 4 reflects the 'buffering' effect of water during both fractional and batch melting.

The value of D_{OH} *(solid–melt)* $= 0.01$ determined from the solubility data is consistent with estimates for D_{OH} *(solid–melt)* based on other geochemical characteristics of MORB. A comparison of the concentration of water in MORB to the concentration of other incompatible elements indicates that D_{OH} *(solid–melt)* during the MORB melting process is similar to that of Ce [27]. Experimental data on the partitioning of Ce between cpx and melt indicate D_{Ce} *(solid–melt)* ≈ 0.01 [48]. The positive correspondence between the values of D_{OH} *(solid–melt)* determined using the olivine solubility data and the geochemistry of MORB provides independent support for the estimates of the depth at which melting initiates (i.e., Fig. 3) and of the depth at which water is removed from the solid residue (i.e., Fig. 4).

An increase in D_{OH} *(solid–melt)* at high pressures also indicates that, even if small amounts of melt are present at depths significantly greater than ~ 100 km beneath mid-ocean ridges (due to the presence of CO_2), such a melt phase would not strongly affect the water content of olivine. For example, at a pressure of 5.0 GPa, $f_{H_2O} \approx 7 \times 10^5$ MPa when water is present; substitution of this value into Eq. (A5) indicates that D_{OH} *(ol–melt)* increases to ~ 0.02 at a depth of ~ 150 km. Therefore, in the presence of $\sim 1\%$ melt, olivine would only lose $\sim 10\%$ of its original water content.

6. Viscosity of the oceanic mantle

The calculations described above indicate that there is enough water in the MORB source to strongly influence its rheological properties. In addition, the low bulk distribution coefficient for water during the MORB melting process indicates that the mantle minerals will be effectively dried out subsequent to melting. To illustrate the implications of these two observations, we show viscosity profiles for the up-

per mantle incorporating a dry rheology, a wet rheology and a rheology that varies with depth due to changes in the water content of the solid assemblage. Based on the seismic anisotropy observed in the shallow oceanic upper mantle (e.g., [49]), dislocation creep is assumed to be the dominant deformation mechanism; further discussion of this choice is made elsewhere (Kohlstedt and Hirth, in prep.).

Because we are extrapolating the viscosities predicted by experimentally determined flow laws to depths of up to 400 km, the influence of pressure on rheology must be taken into account. In the following calculations, we used an activation volume for creep (V) defined by the relationship (e.g., [50]):

$$V = \frac{Q}{T_m}\frac{\mathrm{d}T_m}{\mathrm{d}P} \tag{3}$$

where T_m is the melting temperature of olivine. Values for T_m and $\mathrm{d}T_m/\mathrm{d}P$ were taken from the experimental data of Ohtani and Kumazawa [51]. The value of V determined from Eq. (3) varies from $\sim 15\times10^{-6}$ m^3/mol at low pressure (i.e., <1 GPa) to $\sim 7.5\times10^{-6}$ m^3/mol at 8 GPa; these values are in good agreement with values for V determined by the analysis of dislocation recovery kinetics in olivine [52,53].

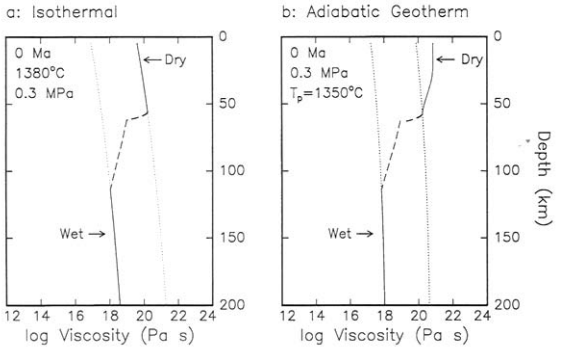

Fig. 5. Viscosity profiles for the mantle beneath a mid-ocean ridge. (a) An isothermal 'mantle' with $T = 1380$°C. (b) An adiabatic mantle with a potential temperature (T_p) of 1350°C. The dotted lines are viscosity relationships calculated for a differential stress of 0.3 MPa using Eq. (2) and Eq. (3) with the wet and dry flow law parameters listed in Table 2. The dashed lines indicate the change in viscosity associated with the change in water content of olivine predicted by the fractional melting relationship in Fig. 4. The increase in viscosity at depths above ~ 65 km in (b) occurs owing to the temperature decrease associated with melting.

Table 2
Flow law parameters for the oceanic upper mantle

Conditions	A (s^{-1} MPa^{-n})	n	Q (kJ/mol)
Dry [a]	4.85×10^4	3.5	535
Wet [b]	4.89×10^6	3.5	515

[a] Parameters based on the flow law of Chopra and Paterson [11]. The value of n is changed from 3.6 to 3.5 (see text for discussion). The value of A was adjusted from 2.88×10^4 to 4.85×10^4 to account for the difference in n. [b] The value of A was calculated for a mantle assemblage containing olivine with 810 H/10^6 Si and based on the assumption that the viscosity of olivine aggregates is inversely proportional to water content.

The viscosity structure at a mid-ocean ridge is illustrated in Fig. 5 for a scenario in which the change in the water content of olivine with depth is affected by fractional melting. The viscosity profiles were calculated for a differential stress of 0.3 MPa using Eq. (2) and Eq. (3) and the flow law parameters summarized in Table 2. To illustrate the effect of pressure on viscosity, there is no increase in temperature with depth in Fig. 5a. The viscosity profiles in Fig. 5b show the effect of an adiabatic temperature gradient as well as the decrease in temperature associated with the latent heat of fusion. The temperature decrease in the melting regime was taken from McKenzie and Bickle [32]. As suggested by Fig. 5b, the effects of pressure and temperature offset each other, resulting in an essentially isoviscous upper mantle between ~ 150 km and 400 km.

The viscosity in the depth interval over which the water content of olivine changes was calculated by assuming that viscosity is inversely proportional to water content; the water contents were taken from the fractional melting curve in Fig. 4. The profiles shown in Fig. 5 illustrate that the viscosity of the mantle prior to the MORB melting event (i.e., at depths greater than ~ 115 km) is on the order of 10^{18} Pa s for a stress of 0.3 MPa (10^{19} Pa s for a stress of 0.1 MPa). Thus the viscosity of the mantle in the MORB source predicted by the application of experimentally determined flow laws is consistent with estimates constrained independently using other geophysical methods (e.g., [54]). In addition, the profiles in Fig. 5b show that, owing to the depletion

of water during the MORB melting event, the viscosity of the mantle increases to $\sim 10^{21}$ Pa s. Between $\sim$ 115 km and 65 km the increase in viscosity is initially gradual because the melt production is 'buffered' by the presence of water. Once the dry solidus is reached and the melt production increases to $\sim$ 1%/kbar (e.g., [32,36]) the remaining water is quickly removed, resulting in an abrupt transition to a dry rheology.

Melt-induced reductions in viscosity were not included in the profiles illustrated in Fig. 5. Experiments on partially molten dunites and lherzolites indicate that the presence of melt does not strongly influence the viscosity of olivine aggregates unless the melt fraction exceeds $\sim$ 0.04 [2,9,17]. Therefore, because geophysical constraints (e.g., [55]) and the geochemical characteristics of MORB and abyssal peridotites suggest that high (i.e. > 0.04) melt fractions are not sustained in the sub-ridge mantle, the omission of melt-induced reductions in the viscosity is reasonable. One exception to this assertion arises due to the influence of melt on grain size. Experimental observations indicate that the presence of melt can result in a decrease in recrystallized grain size [17]. Therefore, it is possible that the onset of melting can result in a decrease in grain size and concomitant change in deformation mechanism. In this case, the viscosity of the mantle may decrease as much as an order of magnitude, even at low melt fractions [17].

The evolution of the 'off-axis' mantle viscosity structure is shown as a function of age in Fig. 6. Viscosity 'contours' are shown in Fig. 6a for a scenario in which the water content of olivine is set 'on-axis' by the MORB melting event. In addition, the viscosity structures of a dry mantle and a 'wet' mantle are shown in Fig. 6b,c to emphasize the effect of the depletion of water from olivine during the MORB melting process. In the calculations used to produce Fig. 6a, the change in the water content of olivine with depth was constrained to be identical to that illustrated in Fig. 4. Therefore the evolution of viscosity with age is only associated with changes in temperature arising from conductive cooling.

An analysis of diffusion data for hydrogen in olivine indicates that the distribution of water with depth remains largely unchanged with age. The characteristics of seismic anisotropy in the ocean basins

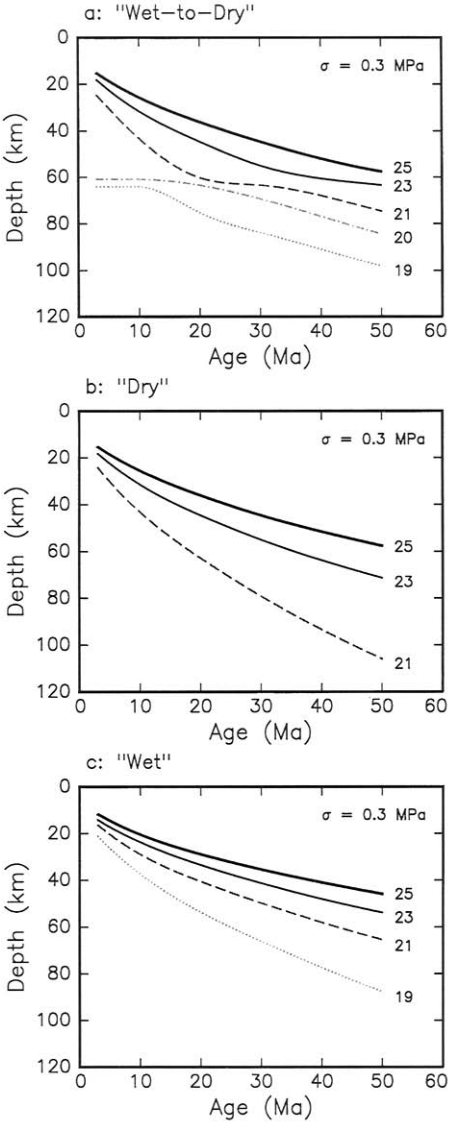

Fig. 6. Viscosity profiles for a conductively cooling mantle half-space as a function of depth and age. Contours of constant log viscosity (in Pa s) are calculated based on the initial viscosity profiles illustrated in Fig. 5. (a) Profiles for a mantle in which the water content of olivine is depleted due to melting at a mid-ocean ridge. (b) A dry mantle. (c) A mantle with a constant water content of 810 H/10^6 Si (i.e., the water content predicted for olivine in the MORB source before the initiation of melting).

indicate that the (010) planes of olivine are oriented approximately parallel to the ocean floor [49]. Diffusion of hydrogen parallel to [010], which is the slowest direction [56], re-hydrates water-depleted

mantle over distances of < 400 m in 150 Ma. Even diffusion parallel to [100], the fastest direction, only results in re-hydration over distances of < 4 km. Thus, even though diffusion of hydrogen in olivine is extremely rapid, measured diffusivities indicate that diffusion alone is insufficient to promote re-hydration of water-depleted mantle present at depths of less than ~ 65 km.

A striking feature of the viscosity structure shown in Fig. 6a is the presence of a high viscosity 'lid' ($\eta > 10^{20}$ Pa s) that extends down to ~ 65 km at young ages. For comparison, as shown in Fig. 6c, without a change in water content viscosities less than 10^{19} Pa s persist to depths of ~ 10 km. The viscosity structure illustrated in Fig. 6a is a consequence of two factors. The dominant effect is the abrupt nature of the transition from wet to dry mantle conditions illustrated in Fig. 4. In addition, because this transition occurs at the relatively large depth of ~ 70 km, conductive cooling does not significantly affect the 10^{19}–10^{20} viscosity contours until ages of ~ 20 Ma.

7. Implications

7.1. Formation of oceanic plates

A comparison of the viscosity structure in Fig. 6a to the 'wet' and dry viscosity structures illustrated in Fig. 6b,c indicates that the thickness of the oceanic plates is controlled by a compositional boundary rather than a thermal boundary or, at least, that the location of the thermal boundary layer is influenced by a compositional boundary. These viscosity structures do not include the effects of temperature changes associated with small-scale convection. Theoretical models suggest that small-scale convection can maintain a temperature on the order of 1380°C at the base of a conductively cooling plate [57], provided that the mantle viscosity is $\leq 10^{19}$ Pa s (e.g., [57,58]). Thus, based on our analysis of mantle viscosity, small-scale convection is expected to occur only in material that has not lost water during the MORB melting process. The deepening of the 10^{19}–10^{20} Pa s viscosity contours in Fig. 6a occurs due to conductive cooling. Conductive cooling at these depths could be retarded by small-scale convection, which should 'flatten' the age versus depth and age versus heat flow relationships (e.g., [59,60]). Thus, the viscosity discontinuity at a depth of ~ 65 km, as illustrated in Fig. 6a, in conjunction with small scale convection, may promote the development of a 'plate-like' geotherm (i.e., a conductive geotherm to a prescribed depth and an adiabatic geotherm below with a thin boundary layer in between).

The presence of a compositional boundary in the oceanic plates has also been proposed based on the results of recent studies on the systematics of off-axis hotspot upwelling and melting [61] and on the seismic velocity structure of the oceanic mantle [62]. Phipps Morgan [61] concludes that a strong and buoyant compositional lithosphere is produced by melting at mid-ocean ridges, that this compositional lithosphere is the principal mechanical barrier to off-axis plume ascent, and that the presence of such a barrier provides an explanation for the observation that the rates of hotspot volcanism appear to be insensitive to the age of the overriding plate.

The seismic velocity model of Gaherty et al. [62] includes a large negative velocity discontinuity ($\sim$ 6% decrease) at a depth of ~ 68 km. The relatively shallow depth of the discontinuity indicates that it is not likely to represent the 'solidus' of the mantle assemblage at these conditions [62]. Based on the analysis presented here of the depletion of water from the solid residue during the MORB melting process, Gaherty et al. conclude that this discontinuity represents the fossilized lower boundary of the melt extraction zone. In this case, the most likely explanation for the decrease in velocity is through the effect of water on anelastic relaxation suggested by Karato [63]. In Karato's model, if Q^{-1}_{dry} is in the range of 0.02–0.01 (where Q^{-1} describes the rate of energy dissipation of seismic waves), a 6% velocity reduction arises if the dislocation mobility is enhanced by a factor of 300–1000 due to the presence of water. This enhancement of dislocation mobility is the same as the water-induced enhancement of creep rate (relative to dry aggregates) that we predict for a mantle with a water content of 810 ± 490 H/10^6 Si. Thus, the magnitude of the velocity decrease described by Gaherty et al. corresponds well with the change in water content of olivine illustrated in Fig. 4 and the effect that this change in water content has on the physical properties of the mantle.

7.2. Evolution of seismic anisotropy

The extraction of water from the mantle assemblage at mid-ocean ridges can also affect the evolution of seismic anisotropy with age. Nishamura and Forsyth [49] illustrate that seismic anisotropy extends to depths of ~ 200 km near the East Pacific Rise, but shoals to ~ 100 km below regions where the seafloor is older than 80 m.y. There is considerable uncertainty in the exact values of these depths and complications that arise from interference between 'fossilized' anisotropy and dynamic anisotropy should be noted. Nonetheless, this observation suggests that the depth limit of fossilized seismic anisotropy in the ocean basins is controlled by the depth to which small-scale convection can occur. Small-scale convection can disrupt the accumulated finite strain of the mantle assemblage and therefore the olivine LPO [49,64]. Thus, if small-scale convection only occurs in the wet regions of the mantle, it follows that the depth limit of fossilized seismic anisotropy could be a manifestation of a mantle viscosity structure that is controlled by the extraction of water at mid-ocean ridges, rather than a change in deformation mechanism from dislocation to diffusion creep.

7.3. Melt extraction at mid-ocean ridges

The strong influence of water on the viscosity of olivine aggregates provides an explanation of how melt migration becomes focused to mid-ocean ridges. As illustrated in Fig. 5, the viscosity of the mantle directly beneath a ridge axis may be on the order of 10^{21} Pa s, owing to the removal of water from olivine during the melt extraction process. This observation indicates that melt migration can be focused to the ridge axes (i.e., the neovolcanic zone) as a result of a pressure gradient produced by corner-like flow [65,66]. Such a hypothesis has previously been questioned because the viscosity required to produce a lateral pressure gradient large enough to affect melt migration in the absence of an anisotropic permeability structure (i.e., $\sim 10^{21}$ Pa s) is significantly greater than that (i.e., $\sim 10^{19}$ Pa s) needed to satisfy other geophysical constraints (e.g., [66]). However, it is apparent that the high viscosity region beneath the ridge axis can be underlain by an upper mantle with a viscosity low enough to satisfy the other geophysical constraints (see also [61]).

8. Conclusions

(1) A re-evaluation of published rheological data indicates that the viscosity of olivine aggregates is reduced by a factor of ~ 140 in the presence of water at a confining pressure of 300 MPa and that the influence of water on viscosity depends on the concentration of water in olivine.

(2) An analysis of solubility data for water in mantle minerals indicates that there is 810 ± 490 $H/10^6$ Si in olivine in the MORB source region. This amount of water is greater than the solubility of water in olivine at 300 MPa, indicating that the viscosity of the mantle in the MORB source region is a factor of $\sim 500 + 300$ less than that of dry olivine aggregates.

(3) The relationships for the solubility of water in mantle minerals are used in conjunction with other petrological constraints to calculate the depth at which melting initiates beneath mid-ocean ridges. These calculations suggest that melting begins at a depth of ~ 115 km, providing a possible explanation for the 'garnet signature' in MORB. However, the amount of water in the MORB source is not sufficient to significantly affect the total amount of melt produced. The solubility data also suggest that the bulk partition coefficient for water increases with increasing pressure (i.e., depth). A positive correspondence between the predicted bulk distribution coefficient and the trace element composition of MORB supports our conclusions reached on the basis of the solubility data.

(4) The extraction of water from olivine during the MORB melting process can result in a mantle viscosity on the order of 10^{21} Pa s in the region directly beneath a mid-ocean ridge. This observation indicates that the viscosity beneath ridges may be high enough to produce lateral pressure gradients capable of focusing melt migration to the ridge axis. At depths greater than ~ 70 km, the viscosity is predicted to be between ~ 10^{18} and 10^{19} Pa s due to the presence of water in olivine.

(5) A sharp discontinuity in mantle viscosity can arise due to the extraction of water from olivine in

the mid-ocean ridge environment. This observation indicates that the thickness of oceanic plates is defined by a compositional rather than a thermal boundary layer, or at least that the location of a thermal boundary layer is strongly influenced by a compositional boundary. A viscosity structure that is controlled by the extraction of water from olivine at mid-ocean ridges can strongly influence the evolution of seismic anisotropy and the mantle geotherm with increasing age.

Acknowledgements

This research was funded by NSF Grants EAR-9405845 (G.H.) and EAR-9405470, EAR-9526925, and OCE-9529744 (D.L.K.). We thank Don Forsyth, Glenn Gaetani, Jim Gaherty, Harry Green, Stan Hart, Greg Houseman, Tom Jordan, Shun Karato, Peter Kelemen, Steve Mackwell, Peter Molnar, Marc Parmentier and Nobu Shimizu for numerous stimulating discussions throughout the evolution of this project. In addition, we thank Jan Tullis and Steve Mackwell for providing comments on the submitted manuscript and David Bell, Jason Phipps Morgan, and an anonymous reviewer for their thoughtful official reviews that aided us in clarifying our arguments. *[CL]*

Appendix A

The water content of olivine during fractional melting is calculated using the relationship [67]:

$$\frac{C_{OH}(ol)}{C^{\circ}_{OH}(ol)} = \left[1 - \frac{MF}{D_{OH}(solid\text{–}melt)}\right]^{\left(\frac{1}{F}-1\right)} \quad (A1)$$

where $C^{\circ}_{OH}(ol)$ is the initial water content of olivine and F is the degree of melting. The bulk distribution coefficient D_{OH} *(solid–melt)* is defined by the relationship:

$$D_{OH}(solid\text{–}melt) = \sum_i D_{OH}(i\text{–}melt)\, X_i \quad (A2)$$

where D_{OH} *(i–melt)* is the distribution coefficient for water between the ith solid phase and melt, and X_i is the corresponding initial weight fraction of the solid phase. The term M in Eq. (A1) is defined by:

$$M = \sum_i D_{OH}(i\text{–}melt)\, m_i \quad (A3)$$

where m_i is the proportion of the ith phase entering the liquid (i.e., the melt mode).

The value of D_{OH} *(ol–melt)* at the depths where MORB melting initiates is calculated using constraints provided by experimental data for the solubility of water in olivine. At 1100°C, the solubility of water in olivine is follows the relationship:

$$C_{OH}(ol) = A_{ol} f^{n}_{H_2O} \exp\left(\frac{-P\Delta V_{ol}}{RT}\right) \quad (A4)$$

where $A_{ol} = 1.1$ H/10^6 Si/MPa, $n = 1$ and $\Delta V_{ol} = 10.6 \times 10^{-6}$ m^3/mol [5]. Assuming that the solubility of water in MORB follows a similar relationship with $n = 1/2$ and that $\Delta V_{melt} \approx \Delta V_{ol}$, D_{OH} *(ol–melt)* at high pressure can be determined by:

$$D_{OH}(ol - melt) = f(P) = \frac{C_{OH}(ol)}{C_{OH}(MORB)}$$

$$= \frac{A_{ol}}{A_{MORB}} f^{1/2}_{H_2O} \quad (A5)$$

At a pressure of 300 MPa, $f_{H2O} \approx 300$ MPa; therefore substitution of D_{OH} *(ol–melt)* = 0.0004 into Eq. (A5) gives $A_{MORB} = 4.8 \times 10^4$ H/10^6 Si/MPa$^{1/2}$. Finally, substitution of this value for A_{MORB} back into Eq. (A5) for a pressure of 2.5 GPa, where $f_{H2O} \approx 2.4 \times 10^4$ MPa [47], gives D_{OH} *(ol–melt)* ≈ 0.003. The melt mode used in Eq. (A3) was taken from [48].

References

[1] S.-I. Karato, Does partial melting reduce the creep strength of the upper mantle?, Nature 319, 309–310, 1986.
[2] G. Hirth and D.L. Kohlstedt, Experimental constraints on the dynamics of the partially molten upper mantle: Deformation in the diffusion creep regime, J. Geophys. Res 100, 1981–2001, 1995.
[3] D.R. Bell and G.R. Rossman, Water in the Earth's mantle: the role of nominally anhydrous minerals, Science 255, 1391–1397, 1992.
[4] Q. Bai and D.L. Kohlstedt, Substantial hydrogen solubility in

olivine and implications for water storage in the mantle, Nature 357, 672–674, 1992.
[5] D.L. Kohlstedt, H. Keppler and D.C. Rubie, Solubility of water in the α, β and γ phases of $(Mg,Fe)_2SiO_4$, Contrib. Mineral. Petrol. 123, 345–457, 1996.
[6] S.-I. Karato and P. Wu, Rheology of the upper mantle: A synthesis, Science 260, 771–778, 1993.
[7] R.S. Hitchings, M.S. Paterson and J. Bitmead, Effects of iron and magnetite addition in olivine–pyroxene rheology, Phys. Earth Planet. Inter. 55, 277–291, 1989.
[8] T. Tullis, F. Horowitz and J. Tullis, Flow laws of polyphase aggregates from end member flow laws, J. Geophys. Res. 96, 8081–8096, 1991.
[9] D.L. Kohlstedt and M.E. Zimmerman, Rheology of partially molten mantle rocks, Annu. Rev. Earth Planet. Sci. 24, 41–62, 1996.
[10] J.D. Blacic, Effect of water in the experimental deformation of olivine, in: Flow and Fracture of Rocks, H.C. Heard, I.Y. Borg, N.L. Carter and C.B. Raleigh, eds., Am. Geophys. Monogr. 16, 109–115, 1972.
[11] P.N. Chopra and M.S. Paterson, The role of water in the deformation of dunite, J. Geophys. Res. 89, 7861–7876, 1984.
[12] S.-I. Karato, M.S. Paterson and J.D. FitzGerald, Rheology of synthetic olivine aggregates: influence of grain size and water, J. Geophys. Res. 91, 8151–8176, 1986.
[13] P.N. Chopra and M.S. Paterson, The experimental deformation of dunite, Tectonophysics 78, 453–473, 1981.
[14] B. Evans, J.T. Fredrich and T.-F. Wong, The brittle–ductile transition in rocks: Recent experimental and theoretical progress, in: The Brittle–Ductile Transition in Rocks, The Heard Volume, A. Duba, W.B. Durham, J.W. Handin and H. Wang, eds., Am. Geophys. Monogr. 56, 1–21, 1990.
[15] Q. Bai, S.J. Mackwell and D.L. Kohlstedt, High-temperature creep of olivine single crystals: 1. Mechanical results for buffered samples, J. Geophys. Res. 96, 2441–2463, 1991.
[16] S.J. Mackwell, D.L. Kohlstedt and M.S. Paterson, The role of water in the deformation of olivine single crystals, J. Geophys. Res. 90, 11,319–11,333, 1985.
[17] G. Hirth and D.L. Kohlstedt, Experimental constraints on the dynamics of the partially molten upper mantle: 2. Deformation in the dislocation creep regime, J. Geophys. Res. 100, 15,441–15,449, 1995.
[18] R.S. Borch and H.W. Green II, Deformation of peridotite at high pressure in a new molten salt cell: Comparison of traditional and homologous temperature treatments, Phys. Earth Planet. Inter. 55, 269–276, 1989.
[19] D.L. Kohlstedt, B. Evans and S.J. Mackwell, Strength of the lithosphere: Constraints imposed by laboratory experiments, J. Geophys. Res. 100, 17,587–17,602, 1995.
[20] T.E. Young, H.W. Green II, A.M. Hofmeister and D. Walker, Infrared spectroscopic investigation of hydroxyl in β-$(Mg,Fe)_2SiO_4$ and coexisting olivine: Implications for mantle evolution and dynamics, Phys. Chem. Miner. 19, 409–422, 1993.
[21] C.W. Burnham, The importance of volatile constituents, in: The Evolution of the Igneous Rocks, J.S. Yoder Jr., ed., pp. 439–482, Princeton Univ. Press, Princeton, N.J., 1979.
[22] T.W. Sisson and T.L. Grove, Experimental investigations of the role of H_2O in calc-alkaline differentiation and subduction zone magmatism, Contrib. Mineral. Petrol. 113, 143–166, 1993.
[23] D.L. Kohlstedt and P.N. Chopra, Influence of basaltic melt on the creep of polycrystalline olivine under hydrous conditions, in: Magmatic Systems, M.P. Ryan, ed., pp. 37–53, Academic Press, San Diego, 1994.
[24] D. Van der Wal, P. Chopra, M. Drury and J Fitz Gerald, Relationships between dynamically recrystallized grain size and deformation conditions in experimentally deformed olivine rocks, Geophys. Res. Lett. 20, 1479–1482, 1993.
[25] D. Van der Wal, Deformation processes in mantle peridotites, Ph.D. Thesis, Univ. Utrecht, 1993.
[26] P.J. Michael, The concentration, behavior and storage of H_2O in the suboceanic upper mantle: Implications for mantle metasomatism, Geochim. Cosmochim. Acta 52, 555–566, 1988.
[27] P. Michael, Regionally distinctive sources of depleted MORB: Evidence from trace elements and H_2O, Earth Planet. Sci. Lett. 131, 301–320, 1995.
[28] J.E. Dixon, E. Stolper and J.R. Delaney, Infrared spectroscopic measurements of CO_2 and H_2O in Juan de Fuca Ridge basaltic glasses, Earth Planet. Sci. Lett. 90, 87–104, 1988.
[29] D. Lizarralde, A. Chave, G. Hirth and A. Schultz, Northeastern Pacific mantle conductivity profile from long-period magnetotelluric sounding using Hawaii-to-California submarine cable data, J. Geophys. Res. 100, 17,837–17,854, 1995.
[30] Q. Bai, Z.-C. Wang, G. Dresen, S. Mei and D.L. Kohlstedt, Solubility and stability of hydrogen in diopside single crystals, in: Trans. Am. Geophys. Union, Fall Meeting Suppl. 75, 652, 1994.
[31] P.F. Dobson, H. Skogby and G.R. Rossman, Water in boninite glass and coexisting orthopyroxene: concentration and partitioning, Contrib. Mineral. Petrol. 118, 414–419, 1995.
[32] D. McKenzie and M.J. Bickle, The volume and composition of melt generated by extension of the lithosphere, J. Petrol. 29, 625–679, 1988.
[33] A.B. Thompson, Water in the Earth's upper mantle, Nature 358, 295–302, 1992.
[34] D. Canil and C.M. Scarfe, Phase relations in peridotite + CO_2 systems to 12 GPa: Implications for the origin of kimberlite and carbonate stability in the Earth's upper mantle, J. Geophys. Res. 95, 15,805–15,816, 1990.
[35] M.M. Hirschmann and E.M. Stolper, A possible role for garnet pyroxenite in the origin of the "garnet signature" in MORB, Contrib. Mineral. Petrol., in press, 1996.
[36] E.M. Klein and C.H. Langmuir, Global correlations of ocean ridge basalt chemistry with axial depth and crustal thickness, J. Geophys. Res. 92, 8089–8115, 1987.
[37] Y. Shen and D.W. Forsyth, Geochemical constraints on initial and final depths of melting beneath mid-ocean ridges, J. Geophys. Res. 100, 2211–2238, 1995.

[38] V.J.M. Salters and S. Hart, The hafnium paradox and the role of garnet in the source of mid-ocean ridge basalts, Nature 342, 420–422, 1989.
[39] S.R. Hart, Equilibration during mantle melting: A fractal tree model, in: Proc. Natl. Acad. Sci. USA 90, 11914–11918, 1993.
[40] T. Plank and C.H. Langmuir, Effects of melting regime on the composition of the oceanic crust, J. Geophys. Res. 97, 19,749–19,770, 1992.
[41] N. von Bargen and H.S. Waff, Permeabilities, interfacial areas and curvatures of partially molten systems: results of numerical computations of equilibrium microstructures, J. Geophys. Res. 91, 9261–9276, 1986.
[42] M.J. Daines and F.M. Richter, An experimental method for directly determining the interconnectivity of melt in a partially molten system, Geophys. Res. Lett. 15, 1459–1462, 1988.
[43] N. von Bargen and H.S. Waff, Wetting of enstatite by basaltic melt at 1350°C and 1.0- to 2.5-GPa pressure, J. Geophys. Res. 93, 1153–1158, 1988.
[44] K.T.M. Johnson, H.J.B. Dick and N. Shimizu, Melting in the oceanic upper mantle: An ion microprobe study of diopsides in abyssal peridotites, J. Geophys. Res. 95, 2661–2678, 1990.
[45] M.J. Daines and D.L. Kohlstedt, The transition from porous to channelized flow due to melt/rock reaction during melt migration, Geophys. Res. Lett. 21, 145–148, 1994.
[46] P.B. Kelemen, J.A. Whitehead, E. Aharonov and K.A. Jordahl, Experiments on flow focussing in soluble porous media, with applications to melt extraction from the mantle, J. Geophys. Res. 100, 475–496, 1995.
[47] K.S. Pitzer and S.M. Sterner, Equations of state valid continuously from zero to extreme pressures for H_2O and CO_2, J. Chem. Phys. 101, 3111–3116, 1994.
[48] P.B. Kelemen, N. Shimizu and T. Dunn, Relative depletion of niobium in some arc magmas and the continental crust: partitioning of K, Nb, La and Ce during melt/rock reaction in the upper mantle, Earth Planet. Sci. Lett. 120, 111–134, 1993.
[49] C.E. Nishamura and D.W. Forsyth, The anisotropic structure of the upper mantle in the Pacific, Geophys. J. 96, 203–229, 1989.
[50] J. Weertman, The creep strength of the Earth's mantle, Rev. Geophys. Space Phys. 8, 145–168, 1970.
[51] E. Ohtani and M. Kumazawa, Melting of forsterite Mg_2SiO_4 up to 15 GPa, Phys. Earth Planet. Inter. 27, 32–38, 1981.
[52] D.L. Kohlstedt, H.P.K. Nichols and P. Hornack, The effect of pressure on dislocation recovery in olivine, J. Geophys. Res. 85, 3122–3130, 1980.
[53] S.-I. Karato, D.C. Rubie and H. Yan, Dislocation recovery in olivine under deep upper mantle conditions: Implications for creep and diffusion, J. Geophys. Res. 98, 9761–9768, 1993.
[54] C.H. Craig and D. McKenzie, The existence of a thin low-viscosity layer beneath the lithosphere, Earth Planet. Sci. Lett. 78, 420–426, 1986.
[55] D.W. Forsyth, Geophysical constraints on mantle flow and melt generation beneath mid-ocean ridges, in: Mantle Flow and Melt Generation at Mid-Ocean Ridges, J. Phipps Morgan, D.K. Blackman and J.M. Sinton, eds., Am. Geophys. Monogr. 71, 1–65, 1992.
[56] S.J. Mackwell and D.L. Kohlstedt, Diffusion of hydrogen in olivine: implications for water in the mantle, J. Geophys. Res. 95, 5079–5088, 1990.
[57] B. Parsons and D. McKenzie, Mantle convection and the thermal structure of the plates, J. Geophys Res. 83, 4485–4496, 1978.
[58] D.W. Sparks and E.M. Parmentier, The structure of three-dimensional convection beneath oceanic spreading centers, Geophys. J. Int. 112, 81–91, 1993.
[59] B. Parsons and J.G. Sclater, An analysis of the variation of ocean floor bathymetry and heat flow with age, J. Geophys. Res. 82, 803–827, 1977.
[60] C.A. Stein and S. Stein, A model for the global variation in oceanic depth and heat flow with lithospheric age, Nature 359, 123–129, 1992.
[61] J. Phipps Morgan, The generation of a compositional lithosphere by mid-ocean ridge melting and its effect on subsequent off-axis hotspot upwelling and melting, Earth Planet. Sci. Lett., submitted, 1996.
[62] J.B. Gaherty, T.H. Jordan and L.S. Gee, Seismic structure of the upper mantle in a central Pacific corridor, J. Geophys. Res., in press, 1996.
[63] S.-I. Karato, Effects of water on seismic wave velocities in the upper mantle, Proc. Jpn. Acad. Ser. B 71, 61–66, 1995.
[64] A. Davaille and C. Jaupart, Onset of thermal convection in fluids with temperature-dependent viscosity: Application to the oceanic mantle, J. Geophys. Res. 99, 19,853–19,866, 1994.
[65] M. Spiegelman and D. McKenzie, Simple 2-D models for melt extraction at mid-ocean ridges and island arcs, Earth Planet. Sci. Lett. 83, 137–152, 1987.
[66] J. Phipps Morgan, Melt migration beneath mid-ocean spreading centers, Geophys. Res. Lett. 14, 1238–1241, 1987.
[67] D.M. Shaw, Trace element fractionation during anatexis, Geochim. Cosmochim. Acta 34, 237–243, 1970.